JMATPRO	Journal of Advanced Materials and Processing 9 (4): 3-12, Autumn 2021 http://jmatpro.iaun.ac.ir 20.1001.1.2322388.2021.9.4.1.3

Research Paper

Effect of Post-Weld Intercritical Annealing on the Microstructure and Tensile Properties of a Gas Tungsten Arc Welded DP700 Steel

Hamid. Ashrafi[1*], Sayyed Erfan Aghili[2]

1. Faculty of Chemical and Materials Engineering, Shahrood University of Technology, Shahrood, 3619995161, Iran

2. Materials Engineering Group, Golpayegan College of Engineering, Isfahan University of Technology, Golpayegan 87717-67498, Iran

ARTICLE INFO

Article history:

Received 2 August 2021
Accepted 12 October 2021
Available online 1 November 2021

Keywords:
Dual-phase steel
Welding
Intercritical annealing
Tensile strength

ABSTRACT

The aim of this study was to investigate the effect of post-weld intercritical annealing (IA) on the microstructure and tensile properties of a gas tungsten arc-welded DP700 steel sheet. In this regard, DP700 steel sheets were first joined using gas-tungsten arc welding. The welded sheet was then annealed at intercritical temperature of 720 °C for 120 s followed by water quenching. Microstructure and microhardness of the as-welded and post-weld heat-treated samples were characterized, as well as tensile properties. Results showed that the microstructure varied from ferrite-tempered martensite in the subcritical heat affected zone to a mixture of bainite, Widmanestatten ferrite, ferrite-carbide aggregate and grain boundary ferrite in the fusion zone. This heterogeneity in the microstructure led to the formation of hardened and softened zones across the welded joint. Strain localization in the softened zone during tensile testing resulted in a joint efficiency of ~ 81% and early fracture. After post weld IA, dual phase microstructures comprising of ferrite and martensite, with different sizes and morphologies, were formed across the welded joint. This new microstructure resulted in the elimination of hardened and softened zones, which in turn led to high joint efficiency of ~ 98%.

Citation: Ashrafi, H., Aghili, S.E., (2021) Effect of Post-Weld Intercritical Annealing on the Microstructure and Tensile Properties of a Gas Tungsten Arc Welded DP700 Steel, Journal of Advanced Materials and Processing, 9 (4), 3-12. Dor: 20.1001.1.2322388.2021.9.4.1.3

[*] **Corresponding Author**
E-mail address: hashrafi@shahroodut.ac.ir

1. Introduction

Dual-phase (DP) steels are the most widely used grade of advanced high strength steel family. Their microstructure is usually composed of ~ 10-40 vol.% of hard martensite islands embedded in a soft and ductile ferrite matrix [1, 2]. This unique microstructure provides an excellent combination of mechanical properties such as high ultimate tensile strength (UTS), good formability, high initial work hardening rate, and low yield strength (YS) to UTS ratio [3, 4]. These mechanical properties make DP steels suitable candidates for use in auto body structures [5].

The structural parts of automobiles are joined by welding, usually resistant spot welding, after completing forming processes [6, 7]. However, there is also a tendency to use tailored welded blanks (TWBs) in the forming processes. TWB's are made of multiple sheets with different materials, strengths, or thicknesses that are butt welded together in a single plane, after which the weldment is stamped into the desired shape [8-10]. One of the main factors affecting the forming behavior of a TWB is material property change in different zones of the weld. Many welding techniques such as inert tungsten gas [11], gas metal arc welding [12], plasma arc welding [13], laser welding [14], and friction stir welding [15-17] have been used for the welding of DP steel sheet blanks. Studies have shown that the formation of a softened zone as a result of the tempering of the martensite in the sub-critical heat affected zone (SCHAZ) and hardening of the fusion zone (FZ) as a result of the fast cooling rate during welding are two serious challenges of DP steels during welding. Panda et al. [18] studied the effect of the softened zone on the formability of laser-welded blanks of DP steels. They concluded that the formability of the welded blanks is lower than that of the respective parent metals, owing to strain localization in the softened zone and a failure mode close to the plane strain condition. Bandyopadhyay et al. [19] observed a fully martensitic microstructure in the FZ of laser-welded DP600 and DP980 steels sheets, which resulted in an early fracture during the Ericksen cupping formability test. It has been demonstrated that in a constant martensite volume fraction, the width of the softened zone and the degree of softening in DP steels increases with increasing the weld heat input. There is also a minimum time that is needed to initiate the softening [20, 21]. Therefore, some researchers tried to use low heat input welding to minimize or eliminate the softened zone. It has been shown by Huan et al. [22] that softening can be eliminated in the low strength grade DP590 steel by minimizing the heat input during laser welding. However, they stated that the formation of a hardened zone is unavoidable. They also observed that the fracture began in the FZ during the Ericksen test.

In an attempt to eliminate the softened zone in the welded sheets of high-strength DP steels, Wei et al. [23] used local cooling during laser welding of DP780 and DP980 steels. They reported that the local cooling could significantly improve the formability of the laser-welded blanks of DP steels. However, the FZ and inner HAZ with low ductility becomes earlier fracture location, reducing the formability of the weldment compared to that for the respective BM. However, the above literature review focused on the laser welding of DP steels, while in the DP steels welded by other welding methods such as tungsten inert gas welding [11], plasma arc welding [13], and friction stir welding [15-17], similar results have been reported.

So far, no method that can eliminate both the softening and the hardening during the welding of DP steels has been proposed in the literature. One simple solution that can eliminate the aforementioned disadvantages and has not been considered yet is post-weld intercritical annealing (PWIA). This solution can be especially useful when two sheets of DP steel of a similar grade with different thicknesses have to be butt-welded together in a single blank before press forming. Therefore, this study aimed to investigate the effect of short-term IA on the microstructure, and tensile properties of a gas-tungsten arc (GTA) welded DP700 steel. For this purpose, DP700 steel sheets were first butt-welded together using gas-tungsten arc welding (GTAW). Then the weldment underwent a short PWIA to eliminate the heterogeneity of the microstructure. Finally, microstructure and mechanical properties of both the as-welded and PWI-annealed samples were studied to analyze the effect of PWIA.

2. Experimental procedure

The material used in this research was a 2 mm thick sheet of DP700 steel with the chemical composition listed in Table 1.

Table 1. Chemical composition (wt.%) of the DP700 steel sheet used in this study

C	Mn	Si	S	P	Ni	Mo	Cu	V	Al	Co	Nb	Zr	Fe
0.18	1.25	0.2	0.01	0.011	0.015	0.019	0.019	0.02	0.073	0.045	0.023	0.011	Bal.

Samples with dimensions of 150 mm × 40 mm × 2 mm were cut from the as-received sheet for performing welding. Before welding, the samples were mechanically and chemically cleaned to avoid any source of contamination that could produce weld defects. In one pass, the samples were then square

butt-welded using manual GTAW (Fronius Magic Wave 2000) in Direct-Current Electrode Negative (DCEN) mode. No filler material was used for the welding operation. The welding current and voltage were 80 A and 8 V, respectively, and a constant welding speed of 1.8 mm/s was also employed. Argon gas of 99.9% purity with a flow rate of 10 Lit/min was used as the shielding and backing gas. Other details of the welding operation can be found elsewhere [24]. The welding parameters of the GTAW process were selected so that a sound weld with minimum heat input could be obtained. After cooling to room temperature, a post-weld intercritical annealing (PWIA) was performed on the welded sample. For this purpose, the weldment was annealed in an electrical furnace at the intercritical temperature of 720° C for 120 s followed by water quenching. The PWIA temperature was the same as the IA temperature of the initial DP700 steel. The time of the IA was the shortest time that could produce a DP microstructure. Microstructural observations were conducted on the cross-section of the as-welded and PW intercritically annealed samples. For this purpose, specimens were cut from the cross-section of the samples followed by standard metallographic sample preparation according to the ASTM E3 standard [25], which included mounting, mechanical grinding to 4000 grit finish, polishing with 0.3 μm alumina suspension, and etching in 2% Nital reagent to reveal the microstructure. The microstructure of the etched specimens was then examined by optical microscopy (OM) in a Nikon EPISHOT 300 optical microscope and scanning electron microscopy (SEM) in a Philips XL30 microscope. Grain size measurements were carried out by the linear intercept method according to the ASTM-E112 standard [26] on the basis of 5 metallography images with different magnifications. The volume fraction of martensite was evaluated by the point-counting method based on the ASTM E562 standard [27] using the Image J software. Microhardness profile was measured along the centerline of the sectioned specimens using a Buhler microhardness tester at a load of 100 g and a dwell time of 10 s according to the ASTM E384 standard [28]. Transverse tensile specimens with the dimensions shown in Figure 1 were cut from the DP700 steel BM, as-welded and PWI-annealed samples and tested at a cross-head speed of 1 mm min-1 using a Hounsfield H50KS machine. The test was repeated three times for each sample to obtain an average for the tensile properties. The tensile test specimens were cut from the as-welded and PWI-annealed samples so that the weld zone (~ 4 mm width) was exactly in the middle of the specimen gauge.

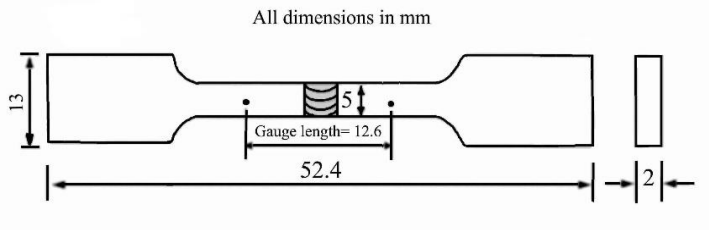

Fig. 1. Dimensions of the tensile tested specimens.

3. Results and discussion

3.1. Microstructural evolution

According to the literature [22], the cross-section of fusion welded DP steels can be divided into six distinct zones: FZ, where the peak temperature is above the melting temperature of steel, coarse-grained HAZ (CGHAZ), in which the peak temperature is well above the critical temperature of A3 (~ 821 °C for the current DP700 steel) and austenite grain growth is intensive, fine-grained HAZ (FGHAZ) in which the peak temperature is just slightly above the A3 temperature, intercritical HAZ (ICHAZ) which experiences a peak temperature between A1 (~ 704 °C for the current DP700 steel) and A3 during welding, sub-critical HAZ (SCHAZ) in which the peak temperature is below the critical temperature of A1, and unaffected BM. Representative microstructures of the aforementioned areas are shown in Figure 2. The microstructure of the DP700 steel BM (Figure 2a) consisted of ~ 28 vol.% of martensite islands (dark) in the ferrite matrix.

The grain size of ferrite was ~ 5 μm, and martensite islands had a mean size of 3.6 μm. SCHAZ (Figure 2b) exhibited a microstructure similar to that in the BM, comprising of martensite and ferrite. Nevertheless, higher magnification SEM images from the microstructure of these two regions, which is shown in Figure 3, revealed that the martensite in the SCHAZ has a broken appearance with the presence of sub-micron particles. These features are characteristics of the partially tempered martensite [29]. As the peak temperature is below the critical temperature of A1, no other microstructural change occurs in this area. In the ICHAZ (Figure 2c), partial austenitization led to the formation of fine pearlite and ferrite besides the tempered martensite. The amount of the newly formed ferrite increased by approaching the A3 isotherm line. The microstructure of the FGHAZ (Figure 2d) consisted of very fine grains of ferrite and pearlite

colonies. In this area, fine austenite grains form at the peak temperature that subsequently transforms to fine ferrite and pearlite upon cooling to room temperature. In the CGHAZ, the peak temperature is so that the austenite grains significantly coarsened upon heating. The large austenite grain size and fast cooling rate in this region promote the formation of displacive transformation products like bainite, Widmanstatten ferrite, and acicular ferrite. In the microstructure of this area (Figure 2e), a mixture of grain boundary (allotriomorphic) ferrite, Widmanstatten ferrite, bainite with ferrite-carbide (FC) aggregate were observed. It is worth mentioning that a finely laminated mixture of ferrite and cementite is known as pearlite, while a ferrite and fine carbide (cementite) mixture is called FC aggregate [30]. Similar microstructural constituents together with an amount of acicular ferrite were observed in the FZ (Figure 2f). However, the microstructure was very coarse in the FZ owing to the full melting during the welding cycle.

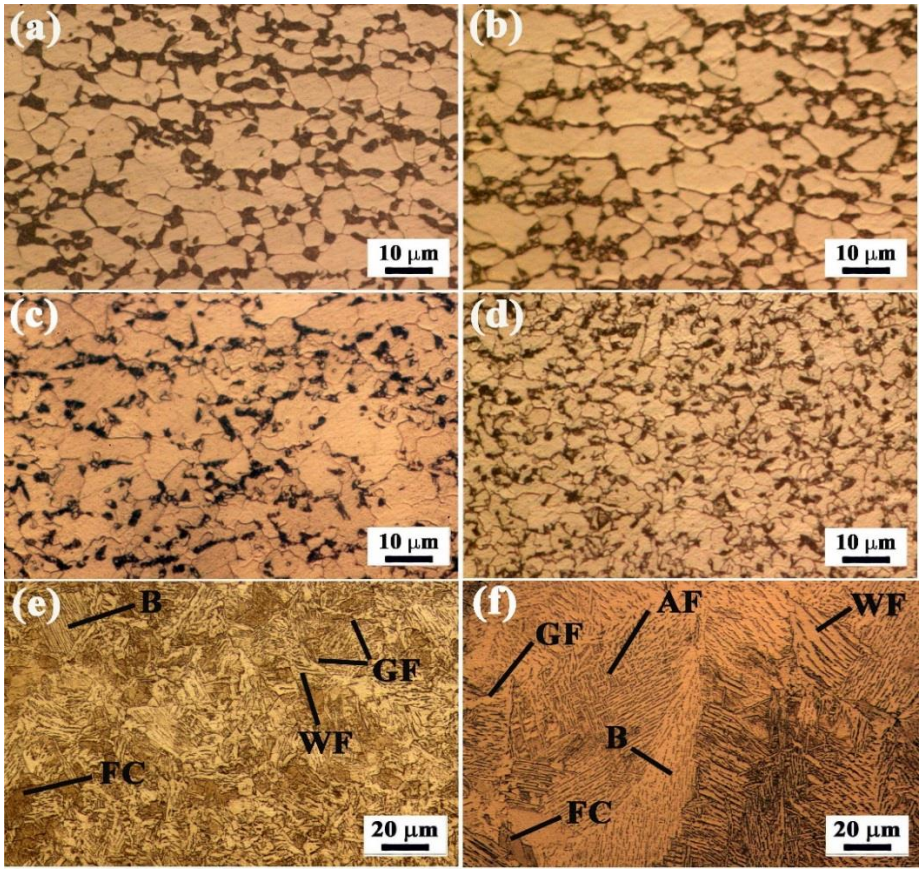

Fig. 2. OM images of the cross-section of the as-welded specimen, (a) BM, showing martensite islands (dark) in the ferrite matrix, (b) SCHAZ, showing partially tempered martensite (dark) in the ferrite matrix, (c) ICHAZ, showing a mixture of tempered martensite and pearlite (dark) in the ferrite matrix, (d) FGHAZ, showing fine pearlite and ferrite, (e) CGHAZ, and (f) FZ. AF: acicular ferrite, B: bainite, FC: ferrite-carbide aggregate, GF: grain boundary (allotriomorphic) ferrite, WF: Widmanestatten ferrite

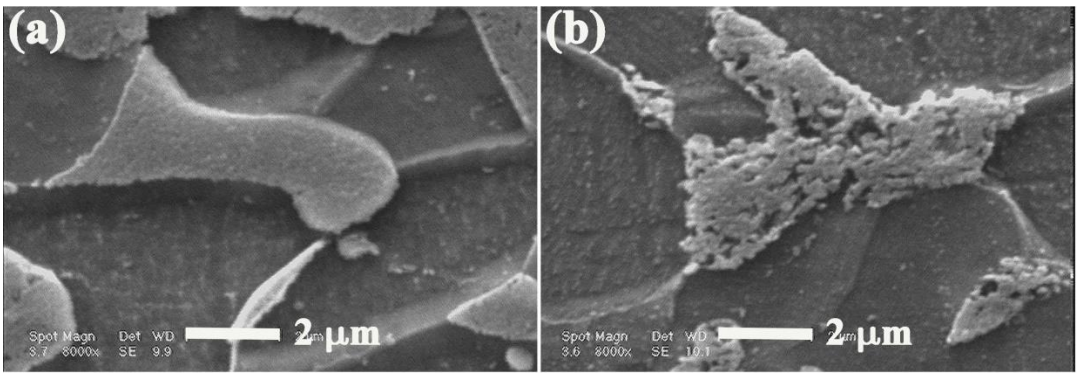

Fig. 3. High magnification SEM image of (a) DP700 steel BM showing martensite islands in the ferrite matrix, and (b) SCHAZ of the as-welded sample showing tempered martensite within the ferrite matrix.

Figure 4 presents the microstructure of different regions across the welded sample after PWIA. The BM (Figure 4a) was comprised of ferrite and martensite, similar to the initial DP700 steel. Moreover, some very small martensite islands were also detected after PWIA. These small islands (~ 1 μm) were mainly located within the ferrite grains. When the initial ferrite-martensite microstructure is reheated to the intercritical temperature, the martensite islands transform to austenite. Because the PWIA temperature was the same as the IA temperature of the BM, and also due to the very short annealing time (120 s), the austenite pools cannot extend into the ferrite phase. At the intercritical temperature, small carbide particles within the ferrite grains can dissolve in the ferrite and form small pools of austenite, as these carbides are suitable sites for austenite nucleation in carbon steels [31].

These austenite pools, which also cannot grow much into the neighboring ferrite, transform to martensite upon quenching to room temperature. Grain boundaries of ferrite are also favorable sites for austenite nucleation [32]. Nevertheless, as can be seen in Figure 4a, many ferrite grain boundaries were free from any martensite island. In fact, owing to the very short time of IA, diffusion of carbon atoms was very limited, and therefore no noticeable change occurred both in the morphology and size of the martensite islands. For the SCHAZ (Figure 4b), the microstructure was very similar to that in the BM. It is clear that the microstructural evolution in these zones is also similar.

In the ICHAZ (Figure 4c), the microstructure was composed of ferrite and martensite, with a bimodal distribution of ferrite grain sizes. This bimodal size distribution was inherited from the as-welded microstructure. During the IA, austenite forms in place of tempered martensite and pearlite. This austenite grows outward in the adjoining ferrite and then transforms to martensite during the water quenching. The FGHAZ (Figure 4d) showed a DP microstructure consisting of martensite islands with a mean size of 3.2 μm distributed in a fine-grained ferrite matrix with an average grain size of ~ 3.3 μm. Martensite particle size was nearly the same as that in the BM, but the ferrite grain size was remarkably reduced. During reheating to the intercritical temperature, austenite forms at pearlitic areas and thickens from there. These areas transform to martensite during quenching. The fine grain size of ferrite in this area was also inherited from the as-welded microstructure.

In the CGHAZ (Figure 4e) and FZ (Figure 4f), elongated martensite particles that were mostly positioned along prior austenite grain boundaries were observed in the microstructure. The ferrite grains in the FZ (~ 40 μm) were significantly coarser than those in the CGHAZ (~ 15 μm). Furthermore, ferrite grains had irregular shapes with jugged boundaries. In the FZ, very large martensite-free areas were seen within the ferrite matrix in comparison to the microstructure of other regions. Moreover, there was a uniform distribution of very fine particles throughout these martensite- free areas. These fine particles, which inevitably had to be cementite particles, were also detected in the CGHAZ. Higher magnification SEM micrographs of the cementite particles in the FZ (Figure 5) revealed their very fine size (< 350 nm). These cementite particles were situated both on prior bainite and Widmanestatten ferrite lath boundaries and inside the ferrite grains. Some of the inter-lath carbides (Figure 5a) appeared to be unaffected by the IA. When the initial microstructure is heated to the intercritical temperature, austenite nucleated on different locations, including prior austenite grain boundaries, carbides on the upper bainite and Widmanestatten ferrite lath boundaries, ferrite-ferrite boundaries, and individual carbide particles [32, 33]. The austenite then transforms to martensite upon water quenching. However, as shown in Figures 4e and 4f, most of the martensite islands were positioned along the prior austenite grain boundaries, while there were a small number of martensite particles at the upper bainite and Widmanestatten ferrite lath boundaries. In fact, the dominant phenomenon in most of the inter-lath carbides was spheroidization. This is in contrast with the fact that carbide particles are suitable nucleation sites for austenite due to their high carbon content [31]. This inconsistency can be explained by considering the grain boundary effect on lowering the critical nucleation energy and the coarse structure of the as-welded sample. In the CGHAZ and FZ of the as-welded sample, a layer of grain boundary (allotriomorphic) ferrite can be seen at the location of prior austenite grain boundaries (Figure 2e and f). It is well understood that ferrite grain boundaries are of higher energy than the bainite and Widmanestatten lath boundaries. Therefore, nucleation of austenite on the ferrite grain boundaries can reduce the total surface energy more effectively than nucleation on the lath boundaries. Furthermore, very short annealing time and coarse microstructure in the CGHAZ and FZ limit the dissolution of cementite particles in the ferrite matrix.

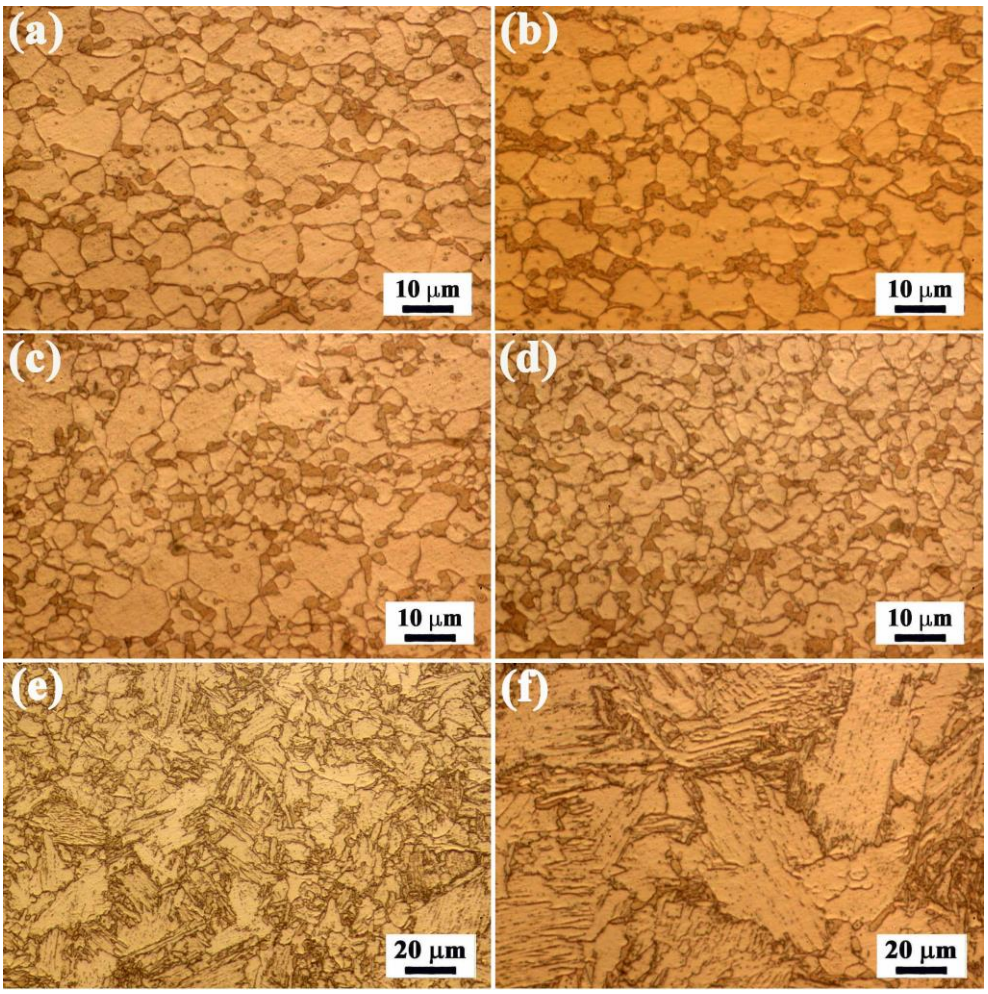

Fig. 4. OM images of the cross-section of PW intercritically annealed sample, (a) BM, (b) SCHAZ, (c) ICHAZ, (d) FGHAZ, (e) CGHAZ, and (f) FZ. The dark phase is martensite, and the bright phase is ferrite.

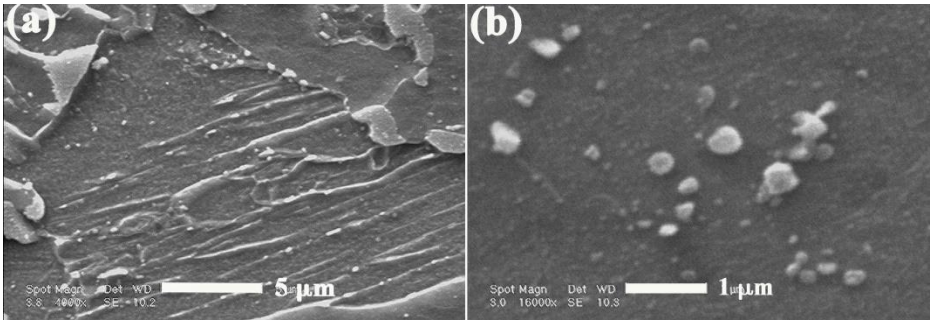

Fig. 5. High magnification SEM images of the FZ after PWIA showing fine particles within the ferrite matrix, (a) particles on the lath boundaries, and (b) particles within the ferrite grains.

3.2. Microhardness measurements

The microhardness profile of the cross-section of the as-welded and PW intercritically annealed samples are shown in Figure 6. The average hardness value of the DP700 steel, represented by a dashed line in Figure 6, was about 222 HV. For the as-welded sample, an area in which the hardness locally drops to values below the BM hardness was observed in the HAZ. The formation of this area, which is known as the softened zone, is attributed to the tempering of the pre-existing martensite. In contrast, in the FZ and CGHAZ, the hardness locally raised to values above the BM hardness. This hardness increase is attributed to the formation of bainite and Widmanestatten ferrite. The hardness distribution was nearly uniform for the PW intercritically annealed sample with a maximum hardness difference of just 30 HV (~ 120 HV for the as-welded sample). This demonstrates the effectiveness of the PWIA in making the hardness uniform throughout the weldment.

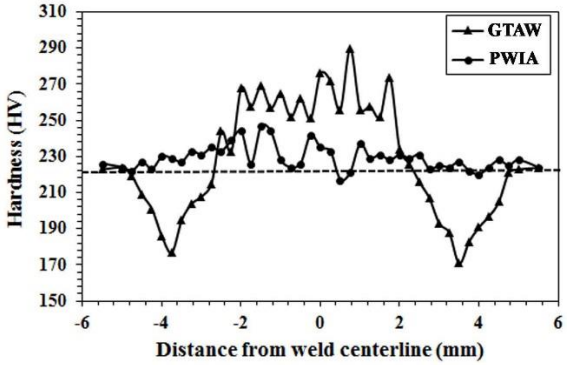

Fig. 6. Microhardness profile of the as-welded (GTAW) and PW intercritically annealed (PWIA) samples. The dashed line specifies the hardness of the DP700 steel BM.

3.3. Tensile properties

Representative engineering stress-strain curves of samples are shown in Figure 7. Table 2 lists a summary of tensile properties. The DP700 steel curve exhibited typical characteristics of the tensile behavior of DP steels, i.e., continuous yielding behavior, low yield ratio, and excellent elongation [34]. After welding, both the UTS and total elongation (TE) were remarkably reduced, while the YS was marginally affected. As can be seen in Figure 7, the welded sample failed in the softened zone. In fact, localization of strain in one of the softened zones during the tensile testing led to the early fracture. The joint efficiency of the welded sample was ~ 81%, which matches well with the ratio of minimum hardness in the HAZ to the hardness of the BM. This indicates that the joint efficiency is strongly affected by the minimum hardness in the HAZ. After PWIA, the UTS was almost fully recovered (joint efficiency of 98%), and the TE was increased to a value comparable to that of the DP700 steel. The recovery of the UTS after PWIA is due to the elimination of the softened zones. The fracture location in the PW intercritically annealed sample also shifted towards the weld centerline, somewhere between the FGHAZ and CGHAZ. Despite the full recovery of UTS, the TE was not fully recovered after PWIA. This can be explained by the fact that although a DP microstructure consisting of ferrite and martensite formed throughout the weldment after PWIA, while the morphology and size of the ferrite grains and martensite islands varied across the weldment. It has been shown in a number of studies [35-37] that martensite morphology, size, and distribution have a considerable effect on the tensile behavior of DP steels. Therefore, the strain distribution was non-uniform along with the gauge of the tensile test specimen, which led to the localization of strain and early fracture.

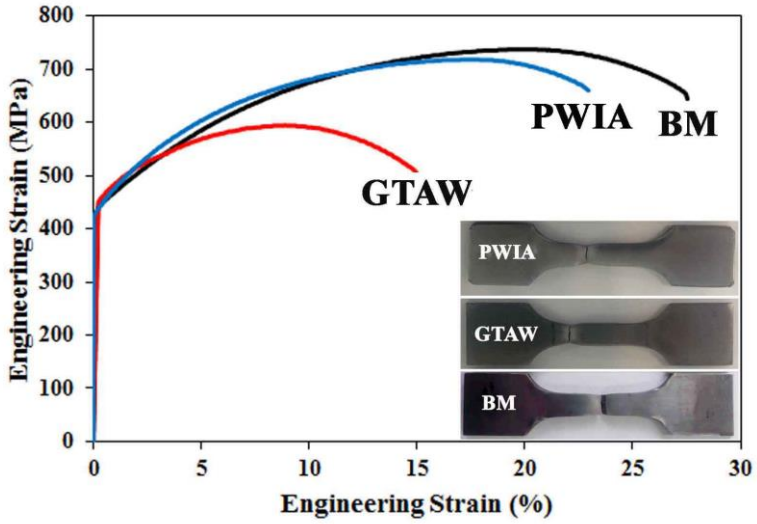

Fig. 7. Engineering stress-strain curves of different samples: BM: DP700 steel base metal, GTAW: as-welded sample, PWIA: post-weld intercritically annealed sample.

Table 2. Summary of tensile properties

Sample	YS, MPa	UTS, MPa	TE, %	Joint efficiency, %
DP700-BM	441 ± 7	736 ± 5	27.56 ± 0.31	-
GTAW	450 ± 12	594 ± 10	15.49 ± 0.7	80.84
PWIA	426 ± 9	722 ± 7	22.9 ± 0.7	98.10

3.4. Work hardening behavior

The work hardening behavior of samples was analyzed based on the Kocks-Mecking procedure [38]. In this approach, the work hardening is assumed to be controlled by the competition between storage and annihilation of dislocations [39]. The variations of instantaneous work hardening rate ($\theta = d\sigma/d\varepsilon$) versus the true stress for different samples are plotted in Figure 8. The gradual decrease of θ with stress or stage III hardening was observed for all samples. The rate of decrease in θ was higher for the as-welded sample. Moreover, a two-stage behavior corresponding to an initial fast decrease in θ with stress followed by a slighter decrease was seen for the PW intercritically annealed sample. It has been claimed that the plastic deformation in DP steels has two stages: plastic deformation of ferrite and co-deformation of ferrite and martensite [40]. It is believed that in the first stage, the deformation of ferrite grains is constrained by the hard martensite islands, resulting in a high initial work hardening rate. As deformation continues, the martensite phase also deforms plastically, exerting less constraining force on the ferrite grains. It is worth mentioning that not all the martensite islands start to deform plastically at once. The plasticity of martensite is determined by its carbon content, size, and morphology [41].

Therefore, by progressing the plastic deformation, more and more martensite islands co-deform with ferrite, which results in a gradual decrease in the work hardening rate. In the as-welded sample (Figure 8b), the rate of decrease in θ was higher than that in the DP700 steel. During the tensile deformation of the as-welded sample, the yielding first occurs in the softened zone, and the plastic deformation is accumulated in this area. Since the tempered martensite in the softened zone is softer than the martensite in the BM, it starts to co-deform with ferrite at lower stresses. Therefore, the constraining force to the ferrite grains decreases more rapidly, and θ reduces at a higher rate. The two-stage work hardening behavior in the PW intercritically annealed sample (Figure 8c) can be attributed to the inhomogeneity of DP microstructures across the tensile teste specimen gauge. The yielding first occurred in the area with the minimum YS during the tensile deformation. This area's work hardens by further plastic deformation until plastic deformation starts in another area. This change in the location of strain accumulation can create a multi-stage work-hardening behavior.

After yielding, the Hollomon equation expresses the flow curve in the uniform deformation stage [42]:

$$\sigma = k\,\varepsilon^{n} \qquad (1)$$

where σ is the true stress, ε is the true strain, *k* is a constant and *n* is the work hardening exponent. The value of *n* has a direct relation with the work hardenability of the material, i.e. its higher value means a higher work hardening rate. A material with a large *n* can more heavily deformed before instability and therefore preferred for processes involving plastic deformation [43]. Table 3 presents the values of work hardening magnitude and *n* for different samples. As can be seen, both values were reduced after welding. PWIA led to a full recovery of the work hardening magnitude and a significant increase in the n value. This means that PWIA can be very effective in the recovery of the formability of the GTA-welded DP700 steel.

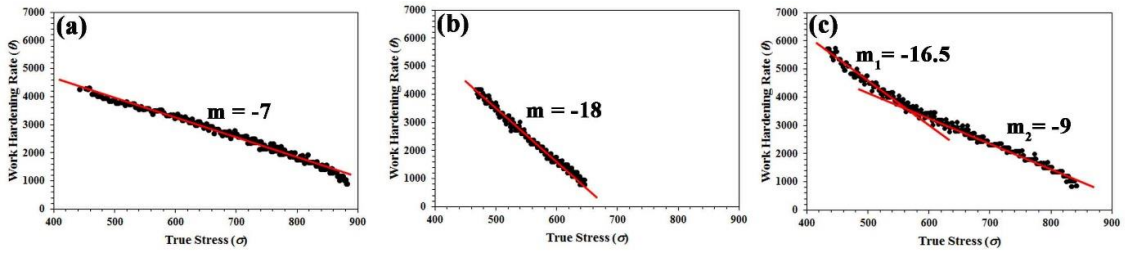

Fig. 8. Work hardening rate plots for (a) DP700 steel, (b) as-welded sample and (c) PW intercritically annealed sample.

Table 3. The values of work hardening magnitude and n for different samples

Sample	Work hardening magnitude, MPa	n
DP700 steel	295	0.23
GTAW	144	0.13
PWIA	293	0.2

4. Conclusions

In the present work, DP700 steel sheets were butt-welded using GTAW. Then a short IA was applied to the weldment. The main conclusions from the results obtained in this study are as follows:

- The DP700 steel joint had a heterogeneous microstructure throughout the weldment. The FZ and CGHAZ showed a microstructure consisting of bainite, Widmanestatten ferrite, acicular ferrite, FC aggregate, and grain boundary (allotriomorphic) ferrite, which resulted in the local hardening. Tempering of martensite in the SCHAZ resulted in forming a softened zone with a minimum hardness significantly lower than that for the BM.
- PWIA led to the formation of a DP microstructure throughout the weldment. However, the morphology and size of ferrite grains and martensite islands varied with distance from the weld centerline. In the FZ and CGHAZ, both equiaxed and fibrous martensite with a uniform distribution of fine cementite particles in a coarse-grained ferrite matrix were observed after IA, which resulted in a remarkable decrease of hardness in the hardened zone. However, in other regions, the microstructure consisted of equiaxed martensite islands distributed on the boundaries of ferrite grains, which resulted in the full elimination of the softened zone.
- The UTS and TE of the DP700 steel significantly reduced after GTAW due to the localization of strain in the softened zone, resulting in early fracture during tensile testing. PWIA resulted in the full recovery of UTS and significant enhancement of TE. The work hardening exponent of the BM was also highly degraded after welding, which mostly recovered after PWIA.

References

[1] S. Nikkhah, H. Mirzadeh, M. Zamani, "Fine tuning the mechanical properties of dual phase steel via thermomechanical processing of cold rolling and intercritical annealing", Mater. Chem. Phys., Vol. 230, 2019, pp. 1-8.

[2] H. Ashrafi, M. Shamanian, R. Emadi, M. Sanayei, F. Farhadi, J.A. Szpunar, "Characterization of microstructure and microtexture in a cold-rolled and intercritically annealed dual-phase steel", J. Mater. Eng. Perform., Vol 30, 2021, pp 7306–7313.

[3] A.K. Srivastava, N.K. Patel, B.R. Kumar, A. Sharma, B. Ahn, "Strength–ductility trade-off in dual-phase steel tailored via controlled phase transformation", J. Mater. Eng. Perform., Vol. 29, 2020, pp. 2783–2791.

[4] M. Maleki, H. Mirzadeh, M. Zamani, "Effect of intercritical annealing on mechanical properties and work-hardening response of high formability dual phase steel", Steel Res. Intl., Vol 89, 2017, pp. 1700412.

[5] S. Pandre, P. Takalkar, N. Kotkunde, S.K. Singh, A.U. Haq, "Influence of temperatures and strain rates on tensile deformation behaviour of dp 590 steel", Materials Today: Proceedings, Vol. 18, 2019, pp. 2603–2610.

[6] H. Zhang, X. Qiu, Y. Bai, F. Xing, H. Yu, Y. Shi, "Resistance spot welding macro characteristics of the dissimilar thickness dual phase steels", Mater. Des., Vol. 63, 2014, pp. 151-158.

[7] F. Hayat, I. Sevim, "The effect of welding parameters on fracture toughness of resistance spot-welded galvanized DP600 automotive steel sheets", Int. J. Adv. Manuf. Technol., Vol. 58, 2012, pp. 1043–1050.

[8] Z. Babić, M. Šljivić, "Application of tailored blanks in the automotive industry", J. Technol. Plast., Vol. 27, 2002, pp. 61-71.

[9] S.K. Panda, V.H.B. Hernandez, M.L. Kuntz, Y. Zhou, "Formability analysis of diode-laser-welded tailored blanks of advanced high-strength steel sheets", Metal. Mater. Trans. A, Vol. 40, 2009, pp. 1955-1967.

[10] Q. Jia, W. Guo, W. Li, Y. Zhu, P. Peng, G. Zou, "Microstructure and tensile behavior of fiber laser-welded blanks of DP600 and DP980 steels", J. Mater. Proc. Technol., Vol. 236, 2016, pp. 73-83.

[11] S. Li, Y. Kang, G. Zhu, S. Kuang, "Microstructure and fatigue crack growth behavior in tungsten inert gas welded DP780 dual-phase steel", Mater. Des., Vol. 85, 2015, pp. 180-189.

[12] A. Ramazani, K. Mukherjee, A. Abdurakhmanov, U.Prahl, M.Schleser, U.Reisgen, W.Bleck, "Micro–macro-characterisation and modelling of mechanical properties of gas metal arc welded (GMAW) DP600 steel", Mater. Sci. Eng. A, Vol. 589, 2014, pp. 1-14.

[13] A.A. Kuril, M. Jagannatham, G.D.J. Ram, S.R. Bakshi, "Transmission electron microscopy studies of plasma arc-welded DP600 dual-phase steel in keyhole mode", Metal. Mater. Trans. A, Vol. 50, 2019, pp. 5689–5699

[14] Q. Jia, W. Guo, W. Li, P. Peng, Y. Zhu, G. Zou, Y. Peng, Z. Tian, "Experimental and numerical study on local mechanical properties and failure analysis of laser welded DP980 steels", Mater. Sci. Eng. A, Vol. 680, 2017, pp. 378-387.

[15] H. Ashrafi, M. Shamanian, R. Emadi, M.A. Sarmadi, "Effect of welding parameters on the microstructure and tensile properties of friction stir-welded DP600 steel", SAE Int. J. Mater. Manuf., Vol. 12, 2019, pp. 165-178.

[16] H. Ashrafi, M. Shamanian, R. Emadi, M.A. Sarmadi, "Comparison of microstructure and tensile properties of dual phase steel welded using friction stir welding and gas tungsten arc welding", Steel Res. Intl., Vol. 89, 2018, pp. 1700427.

[17] M.D. Sameer, A.K. Birru, "Investigations on

microstructural evolutions and mechanical properties of dual-phase 600 steel and AA6082-T6 aluminum alloy dissimilar joints fabricated by friction stir welding", Trans Indian Inst Met Vol. 72, 2019, pp. 353–367.
[18] S.K. Panda, M.L. Kuntz, Y. Zhou, "Finite element analysis of effects of soft zones on formability of laser welded advanced high strength steels", Sci. Technol. Weld. Join., Vol. 14, 2009, pp. 52-61.
[19] K. Bandyopadhyay, S.K. Panda, P. Saha, "Investigations into the influence of weld zone on formability of fiber laser-welded advanced high strength steel", J. Mater. Eng. Perform., Vol. 23, 2014, pp. 1465–1479.
[20] E. Biro, J.R. Mcdermid, J.D. Embury, Y. Zhou, "Softening kinetics in the subcritical heat-affected zone of dual-phase steel welds", Metal. Mater. Trans. A, Vol. 41, 2010, pp. 2348-2356.
[21] M. Xia, E. Biro, Z. Tian, Y.N. Zhou, "Effects of heat input and martensite on haz softening in laser welding of dual phase steels", ISIJ Int., Vol. 48, 2008, pp. 809–814.
[22] P.C. Huan, X.N. Wang, L. Yang, Z. Zheng, Z.R. Hu, M. Zhang, C.J. Chen, "Effect of martensite content on failure behavior of laser welded dual-phase steel joints during deformation", J. Mater. Eng. Perform., Vol. 28, pp. 1801-1809.
[23] C. Wei, J. Zhang, S. Yang, L. Sun, W. Tao, F. Wu, W. Xia, "Improving formability of laser welded automotive dual phase steels with local cooling", Sci. Technol. Weld. Join., Vol. 20, 2015, pp. 145-154.
[24] H. Ashrafi, M. Shamanian, R. Emadi, N. Saeidi, "Microstructure, tensile properties and work hardening behavior of GTA-welded dual-phase steels", J. Mater. Eng. Perform., Vol. 26, 2017, pp. 1414-1423.
[25] ASTM E3, "Standard practice for preparation of metallographic specimens", ASTM, 2017.
[26] ASTM E112, "Standard test methods for determining average grain size", ASTM, 2004.
[27] ASTM E562, "Determining volume fraction by systematic manual point count", ASTM, 2004.
[28] ASTM E384, "Standard test method for microindentation hardness of materials", ASTM, 2016.
[29] V.H.B. Hernandez, S.K. Panda, Y. Okita, N.Y. Zhou, "A study on heat affected zone softening in resistance spot welded dual phase steel by nanoindentation", J Mater Sci, Vol. 45, 2010, pp. 1638–1647.
[30] R. Ghomashchi, W. Costin, R. Kurji, "Evolution of weld metal microstructure in shielded metal arc welding of X70 hsla steel with cellulosic electrodes: A case study", Mater. Charact., Vol. 107, 2015, pp. 317-326.
[31] H. Seyedrezai, A.K. Pilkey, J.D. Boyd, "Effect of pre-ic annealing treatments on the final microstructure and workhardening behavior of a dual-phase steel", Mater. Sci. Eng. A, Vol. 594, 2014, pp. 178-188.
[32] M. Kulakov, W.J. Poole, M. Militzer, "The effect of the initial microstructure on recrystallization and austenite formation in a DP600 steel", Metal. Mater. Trans. A, Vol. 44, 2013, pp. 3564–3576.
[33] P. Li, J. Li, Q. Meng, W. Hu, D. Xu, "Effect of heating rate on ferrite recrystallization and austenite formation of cold-roll dual phase steel", J. Alloy Cmpd., Vol. 578, 2013, pp. 320-327.
[34] H. Ashrafi, M. Shamanian, R. Emadi, N. Saeidi, "Correlation of tensile properties and strain hardening behavior with martensite volume fraction in dual-phase steels", Trans. Indian Inst. Met., Vol. 70, 2017, pp. 1575–1584.
[35] D. Das, P.P. Chattopadhyay, "Influence of martensite morphology on the work-hardening behavior of high strength ferrite–martensite dual-phase steel", J. Mater. Sci., Vol. 44, 2009, pp. 2957–2965.
[36] E. Ahmad, T. Manzoor, M.M.A. Ziai, N. Hussain, "Effect of martensite morphology on tensile dof dual-phase steel", J. Mater. Eng. Perform., Vol. 21, 2012, pp. 382-387.
[37] H. Ashrafi, S. Sadeghzade, R. Emadi, M. Shamanian, "Influence of heat treatment schedule on the tensile properties and wear behavior of dual phase steels", Steel Res. Intl., Vol. 88, 2017, pp. 1600213.
[38] U.F. Kocks, H. Mecking, "Physics and phenomenology of strain hardening: The fcc case", Prog. Mater. Sci., Vol. 48, 2003, pp. 171–273.
[39] G. Sainath, B.K. Choudhary, J. Christopher, E.I. Samuel, M.D. Mathew, "Applicability of voce equation for tensile flow and work hardening behaviour of P92 ferritic steel", Int. J. Press. Ves. Pip., Vol. 132–133, 2015, pp. 1-9.
[40] N. Saeidi, F. Ashrafizadeh, B. Niroumand, "Development of a new ultrafine grained dual phase steel and examination of the effect of grain size on tensile deformation behavior", Mater. Sci. Eng. A, Vol. 599, 2014, pp. 145-149.
[41] M. Mazinani, W.J. Poole, "Effect of martensite plasticity on the deformation behavior of a low-carbon dual-phase steel", Metal. Mater. Trans. A, Vol. 38, 2007, pp. 328–339.
[42] J.H. Hollomon, "Tensile deformation", Am. Inst. Min. Metall. Eng. Trans. Iron Steel Div., Vol. 162, 1945, pp. 268–289.
[43] P. Movahed, S. Kolahgar, S.P.H. Marashi, M. Pouranvari, N. Parvin, "The effect of intercritical heat treatment temperature on the tensile properties and work hardening behavior of ferrite-martensite dual phase steel sheets", Mater. Sci. Eng. A, Vol. 518, 2009, pp. 1-6.